A stochastic hybrid model with a fast concentration bias for chemotactic cellular attraction

Jaume Ojer[a], Álvaro G. López[b], Javier Used[b], Miguel A. F. Sanjuán[b]

[a]*Departament de Física, Universitat Politècnica de Catalunya, Campus Nord B4, 08034 Barcelona, Spain.*
[b]*Nonlinear Dynamics, Chaos and Complex Systems Group. Departamento de Física, Universidad Rey Juan Carlos, Tulipán s/n, 28933 Móstoles, Madrid, Spain*

Abstract

We reproduce the phenomenon of chemotaxis through a hybrid random walk model in two dimensions on a lattice. The dynamics of the chemoattractant is modelled using a partial differential equation, which reproduces its diffusion through the environment from its local sources. The cell is treated discretely and it is considered immersed in a medium with concentration gradients, so that its path is affected by these chemical anisotropies. Therefore, the direction taken in each iteration of the walk is given by a stochastic process that must be biased by the chemical concentrations, giving preference towards the highest values. For this purpose, we model the intensity of the bias by a single parameter, which is related to how much a cell is attracted to a source and, consequently, how efficient this source is with respect to the cellular capture. Since the model is intended for later hybridization with cellular automata models, a thorough quantitative analysis of the parameter space has been carried out. Finally, we also illustrate the efficiency of the cellular capture due to the concentration sources by using stochastic basins of attraction.

1. Introduction

Chemotaxis is a phenomenon based on the directional movement of unicellular organisms, like bacteria or the cells of multicellular organisms, according to the chemical substances concentration in the environment. The first works on chemotaxis were carried out more than one century ago [1, 2], and described the alternation between the stopping and swimming phases in the motion of bacteria, mainly through mobile flagella. If we observe the cell moving in a uniform and isotropic environment in the absence of concentration gradients, the motion follows an erratic path consisting of a swim with arbitrary stops that redirect the cell [3]. Under these conditions, it can not swim in a straight line for a long time, tending to forget with each stop the direction along which it was going [4].

On the other hand, with the existence of chemical gradients due to the presence of concentration sources, the medium becomes anisotropic and the cell performs chemotaxis, since its movement becomes biased by these gradients [5]. Just to recall, by bias in a random walk, we refer to a preference in the choice of the direction of the walk for higher concentration levels of a substance diffused in the environment. Certainly, we can consider that if the cell approaches higher concentrations, it will keep swimming in a straight line for a longer time before stopping [6]. However, if it moves far away from any source, it will tend to stop with higher frequency to take a new direction at random [7], always with the objective of heading another time towards the highest concentrations. Therefore, we can represent this phenomenon through a random walk model [8] in which the time evolves in a discrete way and the cell moves a fixed length during each time interval. By adding a probabilistic bias function to choose the direction of motion, the directional preference towards the location of the sources in the space can be modelled with respect to the chemical gradients [9, 10, 11]. Thus, we reproduce chemotaxis through a biased random walk model [12, 13] given the concentration inhomogeneities in the medium.

This erratic path as chemotactic response is usually viewed as analogous to Brownian motion [14, 15]. Indeed, the fluctuations that the cell experiences along its walk are due to the concentration irregularities present in the medium instead of the impacts by microscopic molecules of its surroundings. There are many works that focus on the extrapolation to the continuum limit representing the temporal evolution in a continuous way [16, 17]. The resulting equations are used macroscopically to describe the cell flux in terms of a chemotactic agent [18]. Therefore, the time variation of the cell density can be determined as a function of the concentration gradients, which are responsible for the aggregation of cells

[19, 20]. However, the usage of hybrid models for chemotaxis in the literature is much more recent and comparatively scarce [21, 22, 23]. These models are being increasingly used in the representation of many biological phenomena [24], specially in the modelling of cancer growth [25, 26, 27]. Hence, the development of hybrid models for chemotaxis that can be easily and efficiently adapted to more complex multiscale models is certainly deserved.

Our main purpose is to design a model that can be efficiently hybridized with specific cellular automata models for tumor growth [26, 27], where immune cells are attracted to the tumor location by chemotaxis during the process of immune cell recruitment [28]. As opposed to previous hybrid models [21, 23], here the cell dynamics is treated discretely [19, 29], while the diffusion of the chemoattractant is modelled by means of continuous partial differential equations [18]. Certainly, the model assumptions must be in accordance with the hypothetical continuum limit above-mentioned [17, 30]. The smaller the spatial dimension is considered, the closer the continuous limit is attained [31]. Consequently, the construction of this analogy to Brownian motion will be done as long as the discretization is accurate enough to accept it [32].

Other works previously designed cellular automata based on nearest neighbors interactions [33, 34, 35, 36], but with a many-body description instead of a single one. In our model, a lattice representing the chemical concentration distribution extends all over the space, and the cell is situated in a certain mesh box. Locally, in a square lattice, the possible random moves of the cell will be towards one of the eight neighboring boxes, except on the borders, where the number can be reduced to five boxes. Throughout the time evolution, the random walk shall go through many sites of the mesh until its capture by an attractive source, according to the imposed concentration bias. Importantly, we have designed a new nonlinear bias function that controls through a single characteristic parameter the influence that the chemical concentration has on the cell's random path. The introduction of this parameter is crucial, since in the context of immune cell dynamics, the bias of a particular cell towards the tumor location might differ from the others. To study this effect, we compute different magnitudes that give us an idea of how intense is the directional preference [37] as a function of the characteristic parameter. In addition, we will discuss the efficiency of the cellular capture in the presence of more than one concentration source.

The paper is organized as follows. In Sec. 2 we describe the biased random walk model that determines the cell's trajectory in the space. We define the concentration map which takes into account the chemical gradients that are present in the non-isotropic medium where the cell is immersed. A probabilistic bias func-

tion that describes the preference for higher concentrations is introduced with the aim of influencing the movement over the lattice. For this purpose, an intensifier parameter is created in Sec. 3, in order to analyze quantitatively the bias intensity and cellular attraction. Furthermore, in Sec. 4 we explore an scenario with two similar concentration sources, which act as chemoattractants in the medium, computing their respective stochastic basins of attraction [38]. Finally, Sec. 5 is devoted as usual to conclusions and discussions related to the new bias function and its efficiency in cellular capture by the sources.

2. Model description and bias construction

2.1. Concentration map

As previously said, we consider the cell immersed in a non-isotropic medium. Therefore, we assume that one or more concentration sources, defined by the density of chemoattractant ρ, create an effective potential U, which spreads all over the two-dimensional space, spanned by the coordinates $\mathbf{x} = (x, y)$. The relationship between the potential and the source is given by Poisson's equation

$$\frac{\partial^2 U(\mathbf{x})}{\partial x^2} + \frac{\partial^2 U(\mathbf{x})}{\partial y^2} + \rho(\mathbf{x}) = 0, \tag{1}$$

where we have assumed that the concentration gradient is stationary, since in the present work we want to focus on fixed environments, in order to more clearly settle the model properties. Further extension of the present model to evolving scenarios is straightforward by simply replacing the partial differential equation describing the reaction and diffusion phenomena of the chemoattractant in the environment. These effects are specially important when the chemoattractants are produced by the attracted cells themselves, since the sources are then in motion as well [39]. The cell heads towards the higher values of U according to the spatial arrangement of the sources. Then, we need to solve this partial differential equation to numerically obtain the effective potential that characterizes the chemotaxis phenomenon. For this purpose, we use a finite-difference method consisting of discrete step approximations for the derivatives. A discretization of the variables is done on a lattice with a uniform spacing h. In two dimensions, both coordinates are equally discretized as $x = ih$ and $y = jh$ with $i = 0, ..., N_x$ and $j = 0, ..., N_y$, respectively. Defining $f(x, y) = f(ih, jh) \equiv f_{ij}$, the two-dimensional function becomes an array of dimension $N_x \times N_y$. Then, Eq. 1 can be written as

$$U_{i+1,j} + U_{i-1,j} + U_{i,j+1} + U_{i,j-1} - 4U_{i,j} + h^2\rho_{i,j} = 0. \tag{2}$$

Therefore, the numerical resolution requires to solve a matrix linear equation, and the number of these equations depends on the step size, namely on N_x and N_y, corresponding to both dimensions of our space.

The discretization also requires a spatial initialization in order to compute the potential over the whole lattice. We impose Dirichlet boundary conditions so that the lattice edges take constant values, while the remaining points are the unknown variables. The specific conditions are as follows:

1. For simplicity, the upper and lower edges are set at a fixed value $U = 1$. This is the normalized lowest value that the potential will take throughout the lattice [26, 27].
2. The left and right edges wrap around. Each mesh row is modelled as a ring, so the cell on the left edge is a neighbor of the cell on the right and vice versa. This creates the perception of an infinite grid and can be appreciated with a cylindrical symmetry rather than the conventional Cartesian mesh.

With regard to the concentration sources, we model them through a mathematical function centered at some point $\mathbf{x}_0 = (x_0, y_0)$ in the space. It is well known that the most general solution to the physical phenomenon of diffusion is a Gaussian [40, 41]. Thereby, a natural function for the source ρ that diffuses through the space could be an exponential in the form

$$\rho(\mathbf{x}) = \rho_0 \exp\left(-\frac{\left(r(\mathbf{x}, \mathbf{x}_0) - R\right)^2}{\sigma^2}\right), \tag{3}$$

where $r(\mathbf{x}, \mathbf{x}_0) = \sqrt{(x - x_0)^2 + (y - y_0)^2}$ and $R = h$ defines its action radius. The exponential width is given by σ^2, whereas ρ_0 is related to the maximum value that the potential reaches.

As stated above, the resolution of the problem to numerically obtain the effective potential implies solving a set of linear equations, where there is one equation for each inner point of the lattice. We use one of the most popular methods to solve the partial differential equation in a matrix form. The successive over-relaxation method explicits the term $U_{i,j}$ of Eq. 2 to find the solution iteratively [42]. The main advantage of this method is that it is diagonally dominant, which ensures a convergence after a certain number of iterations and with a much lower consumption of computational time in comparison with other methods [43]. Unless otherwise indicated, the simulation is carried out in this work utilizing a 100×100 dimensional grid with a uniform integration step of $h = 0.5$.

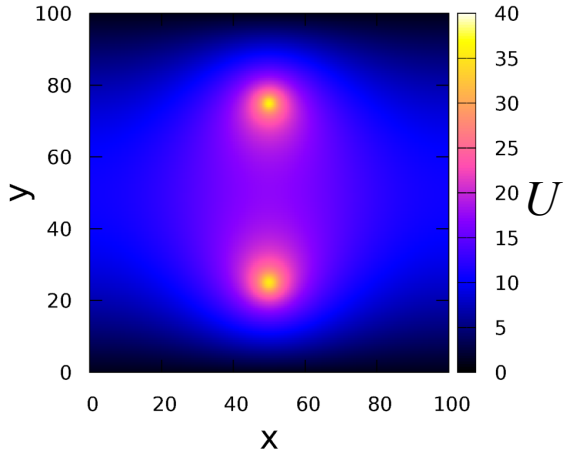

Figure 1: **The effective potential**. Two-dimensional representation of the effective potential, U, in presence of two concentration sources. The exponential model has been used with a depth of $\rho_0 = 10$ and a width of $\sigma = 0.8$ for the upper source in $\mathbf{x}_0 = (50, 75)$, whereas the values $\rho_0 = 6$ and $\sigma = 1.2$ have been used for the lower one in $\mathbf{x}_0 = (50, 25)$.

2.2. Random walk

The mathematical and computational treatment of the cell's path, which is immersed in an anisotropic medium, is based on a biased random walk model [12, 13]. The discrete disposition of the potential leads not only to the fixed step motion of the cell, but also to a reduced number of possibilities to choose a direction of motion in each time step. This casuistry has to be only perceptible zooming in the trajectory, while negligible from a macroscopic viewpoint. This local feature is always present in any computational modelling in which a discretization of space is done [17, 30]. Then, contrary to what is obtained using Brownian motion, the resulting random walk is a discrete jump process that is not self-similar [44]. However, the uniform spacing, h, can be small enough to construct correctly an analogy with a Brownian motion [32]. The mathematical description of the latter is a continuous-time stochastic process in which all directions of motion are possible, so we can achieve this ideal continuity in time reducing the uniform spacing as much as we can [31]. Further information about this convergence in distribution can be found in the literature [45].

The cell's transition from a certain mesh box to another is given only by nearest neighbors (nn). Then, the transition probability is determined through the

characteristic bias of the random walk. Summing over the potential values of the set of nearest neighbors $\{p, q\}$, we define the sampling weight of the cell (i, j) as

$$\omega_{i,j} = \frac{U_{i,j}}{\sum_{(k,l)\in\{p,q\}} U_{k,l}}, \tag{4}$$

so the transition probability to move towards this cell (i, j) can be given by

$$\pi_{i,j} = \frac{\mathcal{F}(\omega_{i,j})}{\sum_{(k,l)\in\{p,q\}} \mathcal{F}(\omega_{k,l})}, \tag{5}$$

where the function $\mathcal{F}$ is what we call the *bias characteristic function*. Similar transition techniques can be found in previous works in the literature [33, 35].

In order to make the transition, the method consists in generating a random number μ, which follows the uniform distribution in the interval $[0, 1]$. We have to determine if this number belongs to an interval given by one of the transition probabilities. If so, the cell moves towards the corresponding mesh box, and so on for each time step. Following the disposition of Fig. 2, this algorithm is also known as the roulette wheel selection [46], which determines the destination box

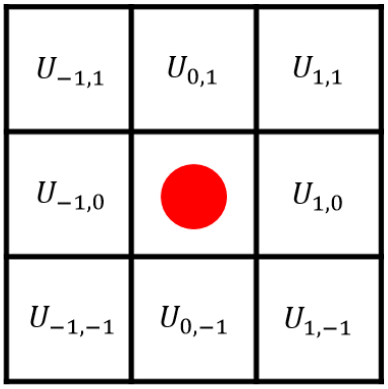

Figure 2: **Nearest neighbors arrangement**. The potential's grid layout under the discretization of space determines the nearest neighbor transition of the cell. This one is located in this image in the center $(0, 0)$ represented by a big red dot. Notice that this arrangement is typical of an inner lattice point because of $nn = 8$. If the cell was on the top or bottom border, then $nn = 5$.

as the first nearest neighbor with indexes (i, j) that satisfies

$$\sum_{(k,l)}^{(i,j)} \pi_{k,l} > \mu. \tag{6}$$

The choice of the bias characteristic function depends on the chemotactic response that we consider. Obviously, this function has to be non-negative since a transition probability is always positive. Another aspect that we have to take into account is bijectivity. Indeed, since transition equiprobability can not exist for different values of $\omega_{i,j}$, each sampling weight must have a different image from the rest of weights. Therefore, the function has to be monotonically increasing. Specifically, the consideration of a cellular attraction by the higher concentrations implies a positive slope throughout the whole interval. In this way, we propose a Gompertz curve as the bias characteristic function of the model, as follows

$$\mathcal{F}(\omega_{i,j}) = \exp\left[-10a \exp\left(-a\omega_{i,j}\right)\right], \tag{7}$$

where a is a positive constant that expresses the intensity of the bias when making the transition movement across the lattice. As we show below in Sec. 4, this nonlinear function allows to control very efficiently the bias of the walk and the cellular capture by the sources, where a single parameter totally controls the deterministic part of the motion in the chemotactic response. Importantly, it is biologically expected that different cells within a tissue present heterogeneous sensitivity

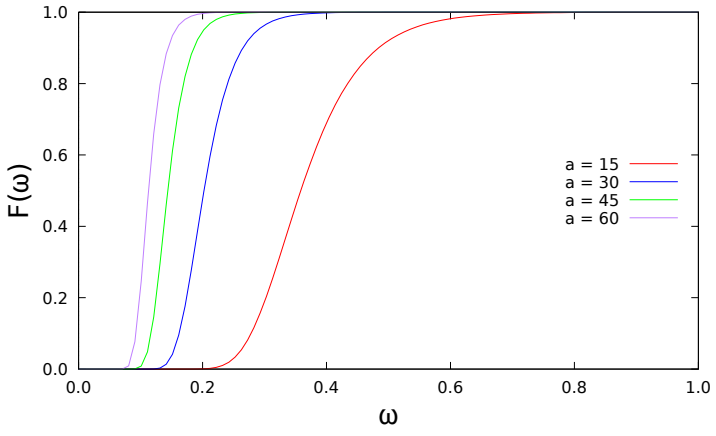

Figure 3: **The bias characteristic function**. Representation of the Gompertz curve depending on the sampling weight. Notice that the value of a not only changes the function's slope but also where the curve takes place regarding ω.

to chemoattractants, since the efficiency of chemotaxis depends on many biological factors at the cell scale. The present parameter has the usefulness of allowing us to model all these complex random phenomena, by simply letting it to fluctuate from one cell to another. The fact that the implementation of the Gompertz curve to represent the bias is so simple and efficient at the same time, makes it one of the best candidates to model the phenomenon of chemotaxis through random walks on a lattice in more complicated computational models [33, 39], which might be already highly time-consuming [26, 27].

For the case of an isotropic medium, the potential would have the same value everywhere, so that an equiprobability would exist with $\omega = 1/nn$ for each nearest neighbor. However, as this can not occur in anisotropic conditions, we can suppose that the highest sampling weight corresponding to the highest concentration achieves greater values. Therefore, if we observe Fig. 3, the value of a for which the curve takes place at greater weights is $a = 15$, whereas for increasing values the curve is given at smaller weights. These considerations provided, we conclude that the lower the constant a, the more intense the bias, and conse-

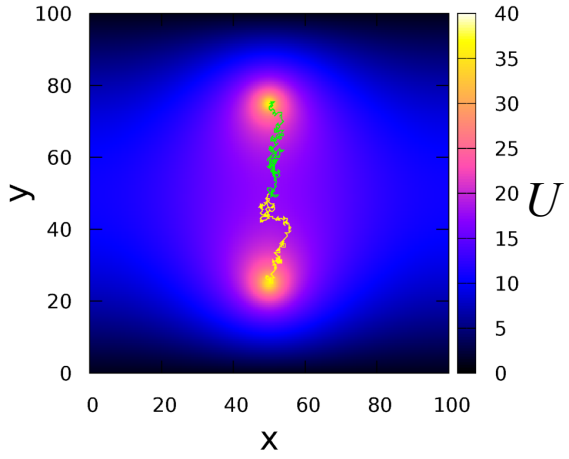

Figure 4: **The biased random walk**. Representation of the same concentration sources as in Fig. 1, but now adding also two biased random walks that are born in the center of the map. Each one is drawn in a different color, green and yellow, in order to differentiate to which source has been attracted. An intensifier parameter of $a = 40$ has been used for the simulation of the paths. Notice that even though both walks start from the same point in space, due to the randomness of the algorithm, they are not captured by the same source.

quently, the more significant the cellular attraction as well.

The strengthening of transition probabilities towards the highest values of the potential, via a nonlinear bias characteristic function like the Gompertz curve, represents an advantage regarding probabilities that are simply proportional to the concentration gradient [34, 36]. Moreover, by controlling the function to enhance only the greatest weights we can practically ignore the lowest concentrations, what can not be achieved for more simple monotonically increasing functions, such as the exponential function or a product of exponentials [35]. This fact allows our model to more efficiently represent the cell capture by the sources.

3. Analysis of the bias function

Definitely, the positive constant appearing in Eq. 7 determines the bias characteristic function. It is the only degree of freedom used to characterize our biased random walk. Thus, a quantitative analysis that classifies each erratic path of the cell according to the value of a is essential to understand the relation between this parameter and the nature of the walk. We use the so-called indexes of motion behavior [37] to study a certain property of the walk, depending on the intensity of the bias.

It is important to bear in mind the stationarity of the potential gradients, and thus, a fixed concentration map while random walks evolve. For this reason, we can analyze the cell's trajectory in function of a but keeping constant source parameters like ρ_0 and σ^2, and not the other way around. Nevertheless, we will set different values of these parameters to know their influence in the motion of the cell.

We use for this section the system's arrangement represented in Fig. 5, with a single concentration source modelled by Eq. 3. Moreover, the cell is initially placed at a fixed distance with respect to the source, with the aim of carrying out a total $N = 10^3$ random walks for each value of the constant a. In this way, we compute a certain index of motion behavior I through the sample mean

$$I(a) = \frac{1}{N} \sum_{k=1}^{N} i_k(a), \tag{8}$$

where i is the index of the k-th random walk, in particular. The analysis is developed through the variation of a, studying the quantitative changes as the probabilistic bias is modified. Then, using two definitions of index of motion, the *shape*

of the biased random walk is analyzed through two properties of the motion behavior: the spatial anisotropy and the tortuosity of the path. For the different values of a, we show the variation of the corresponding index depending on how much spherical and tortuous the walk results.

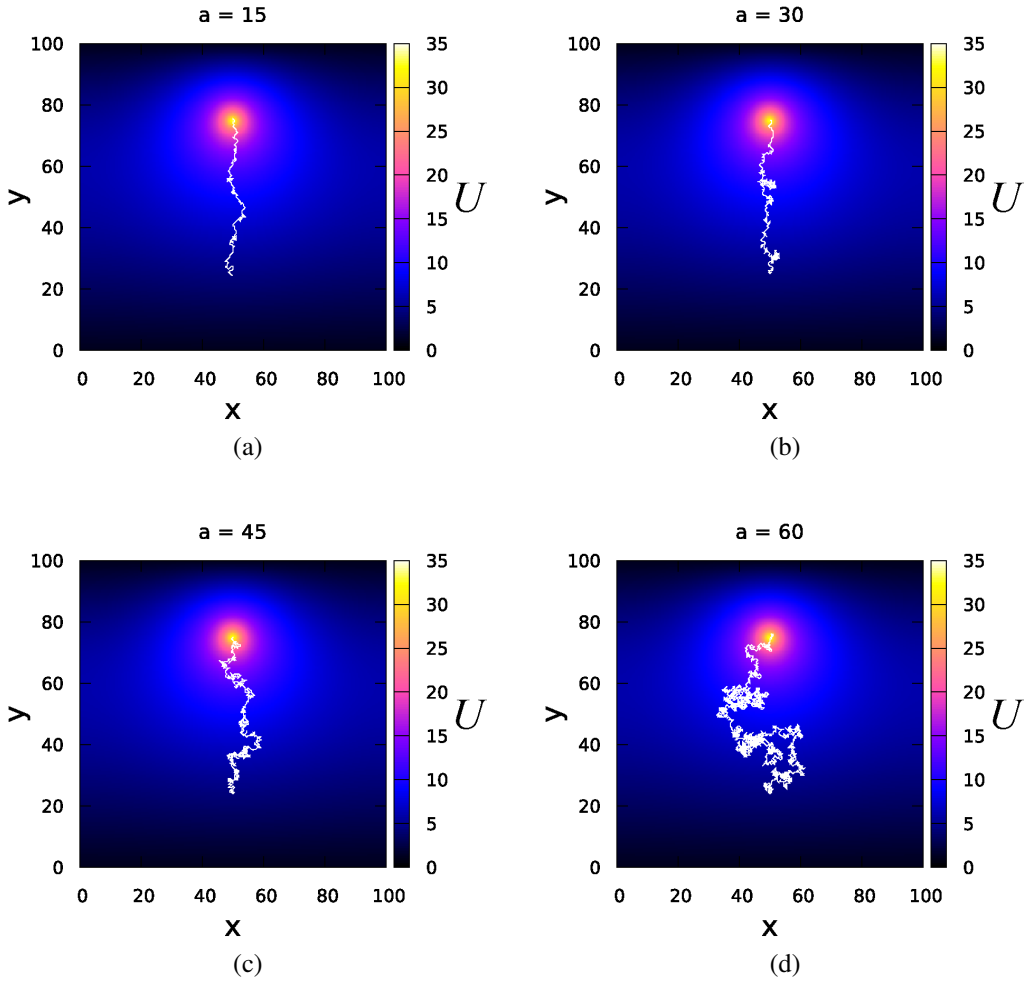

(a) (b) (c) (d)

Figure 5: **The intensity of the bias**. The single concentration source in $\mathbf{x}_0 = (50, 75)$ is modelled using a depth of $\rho_0 = 10$ and a width of $\sigma = 0.8$. As it can be seen, with the cell initially placed at $\mathbf{x}_0 = (50, 25)$, more erratic random walks are obtained for increasing values of a. The aim consists of studying how indices of motion vary as the erraticity of the walks increases, i.e., the bias turns to be less intense.

3.1. Sphericity: anisotropy

For a simple isotropic random walk (unbiased), the statistical distribution of visited points is rotationally symmetric with respect to its origin. However, for a biased random walk, the paths tend to be more elongated due to the predilection for a specific direction. This elongation causes the spherical symmetry to be lost, a particularity given by its spatial anisotropy, which is not a statistical anomaly but a characteristic feature of the random walk. The presence of any bias represents a certain determinism in the motion, since not all directions are equally probable. We then need to describe the size and shape of the walk as a function of the different directions of the motion. Following Ref. [47], the radius of gyration tensor in two dimensions is defined here as

$$G = \begin{pmatrix} \sigma_x^2 & \sigma_{xy} \\ \sigma_{xy} & \sigma_y^2 \end{pmatrix}, \tag{9}$$

where the diagonal and off-diagonal elements are the variances of each two directions and the covariances between them, respectively. The averages here are computed through the number of footprints, what renders a single matrix for each walk.

Notice that Eq. 9 can be regarded as a moment of inertia tensor that equips the walk traced by the cell with the property of a rigid body. Being symmetric and positive-definite, the tensor can be diagonalized by deriving its real and also positive eigenvalues $\lambda_{\pm}$. Defining $\sigma_{\pm} \equiv \sigma_x^2 \pm \sigma_y^2$ and $\Phi^2 \equiv \sigma_-^2 + (2\sigma_{xy})^2$, the eigenvalues can be easily obtained as

$$\lambda_{\pm} = \frac{\sigma_+ \pm \Phi}{2}. \tag{10}$$

These values quantify the average extension of the random walk in each direction. Particularly, under bias the total elongation leads to a direction along which the path is more extended than along the other one. We then refer to it respectively as the expansion direction and the contraction direction, which are effectively orthogonal. Indeed, the eigenvalue λ_+ lying on the expansion direction represents the square of the semi-major axis of the ellipse along which the walk is confined, whereas λ_- lying on the contraction direction that represents at the same time the square of the semi-minor axis. In this way, the intersection point between both semi-axes is the center of the ellipse, which physically can be considered as the center of mass of the walk.

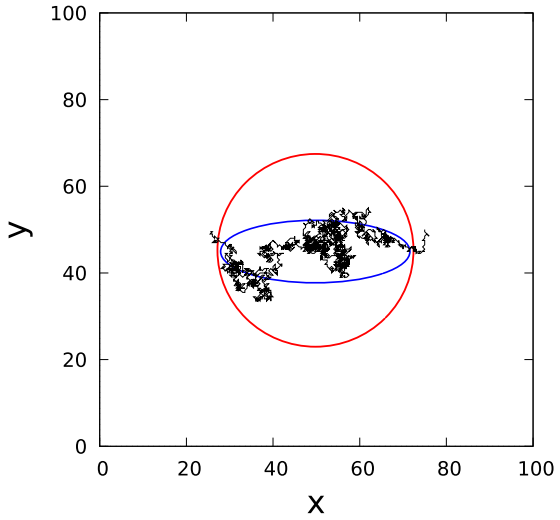

Figure 6: **Sphericity of a random walk**. Confinement of a biased random walk (in black) in an ellipse (in blue) computed through the radius of gyration tensor. A circle (in red) is also drawn, which, using Pythagoras' theorem, has a radius of $R_g = \sqrt{\lambda_+ + \lambda_-}$. To construct the walk, a disposition of the source like in Fig. 5 but with axes switched has been used. An expansion and contraction direction in x-axis and y-axis can be distinguished, respectively.

Now, we can define an index of motion behavior that gives information about the sphericity of the walk. Confining it in an ellipse, if both eigenvalues are similar, the spreading to both directions would be practically equal, and as a consequence the ellipse would be slightly eccentric (high sphericity). If, conversely, there is a great difference between them, the extension is greater on the expansion direction, resulting a very eccentric ellipse (small sphericity). The spatial anisotropy due to this eccentricity is usually defined as the ratio between the eigenvalues with the largest one at the denominator [48]. For an increasing bias, the ellipse would be more and more elongated and, therefore, the ratio would be smaller and smaller. For this reason, it can not be a good indicator of anisotropy, since its value would tend to increase instead of decreasing: the anisotropy is greater in the presence of a spatial preference, i.e., an elongated ellipse, which can be obtained with small values of a for the bias. We propose the ratio between the difference and the sum of both eigenvalues, which, unlike the previous definition, it increases for high eccentricities. Using Eq. 10, the index of motion behavior takes the following simple form

$$\Lambda = \frac{\Phi}{\sigma_+}. \tag{11}$$

We can check from Fig. 7 that not only the bias decreases for an increasing parameter a, but also the index of anisotropy decreases from values close to the

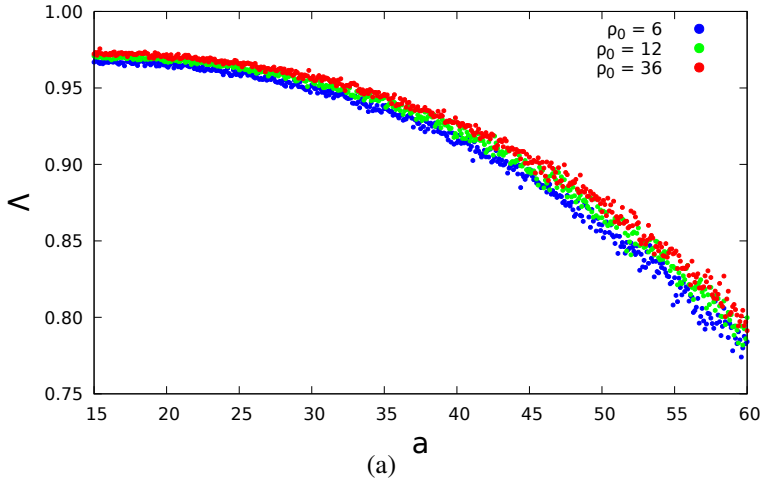

(a)

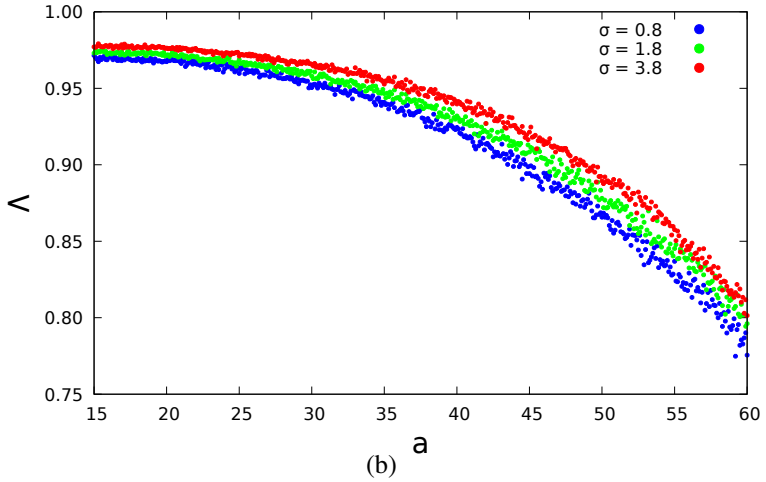

(b)

Figure 7: **The index of anisotropy**. The index clearly decreases for a decreasing bias, which can be achieved increasing the value of a. The random walk then becomes more spherical, with an increasingly shorter expansion direction and longer contraction direction. Using the source disposition of Fig. 5, several values of ρ_0 (top, setting $\sigma = 0.8$) and σ^2 (bottom, with $\rho_0 = 10$) are also included. Every single dot depicted in this figure corresponds to a certain value of the index following the definition of Eq. 8.

unity. This behavior is given according to an increasingly spherical walk, while for an intense bias a high anisotropy is obtained between both directions, i.e., a very elongated ellipse. Furthermore, different values of ρ_0 and σ^2 are considered. We see that greater depths and widths of the concentration source give place also greater anisotropies, since it increases the potential gradient, and then, decreases the sphericity of the walks.

3.2. Tortuosity: intensity use

An important property of any random walk is how erratic it is in a given space and time. The number of twists, turns and tumbles that the path experiences prevents it from being perfectly straight. We refer to this erraticity as the tortuosity, which is an intrinsic property of the walk and should be quantified through an index of motion behavior. The straightness is defined as the ratio between the Euclidean distance from the beginning until the end of the path and the total traveled length $l = Kh$ [49], where K is the total number of iterations required for cell's capture by the source and h the integration step. It is therefore a way to compare the real length of the walk with the shortest possible. Following the disposition of Fig. 5, since this Euclidean distance is always the same regardless of shape of the path, we prefer the intensity use rather than the straightness. The former compares the total length with the square root of the surface that covers the walk's motion [50, 51]. In practice, the calculation of this area is not usually easy, but here we can take advantage of the information provided in Sec. 3.1 and the ellipse in which the walk is confined. Employing the well-known formula for the area of an ellipse and using Eq. 10, the intensity use is defined as

$$IU = \frac{Kh}{\sqrt{\frac{\pi}{2}\sqrt{\sigma_+^2 - \Phi^2}}} \approx \frac{Kh}{\sqrt{\pi\sigma_x\sigma_y}}, \tag{12}$$

where the approximation has been performed if we consider zero correlation between walk steps. From Fig. 8 we note an increasing tendency of the index for a decreasing attractive effect of the source. It is mainly due to the higher number of iterations K in a weaker bias, i.e., a higher traveled length l. On the other hand, an increasing attraction for an intense bias implies a less spherical walk, and therefore a lower surface of the confining ellipse. However, this fact seems to be not more significant than the loss of erraticity, as the ratio decreases for decreasing values of a, as well. Hence, the rise or decrease of iterations proves to be more important than how spherical the walk is, since its total length varies faster and much more than the square root of surface.

Like for the index of anisotropy, we have considered here different values of ρ_0 and σ^2 too. However, their influence does not seem to be now just as important. If we increase the depth of the concentration source, the intensity use decreases but not in a significant way, so the walks become slightly less tortuous. The variation

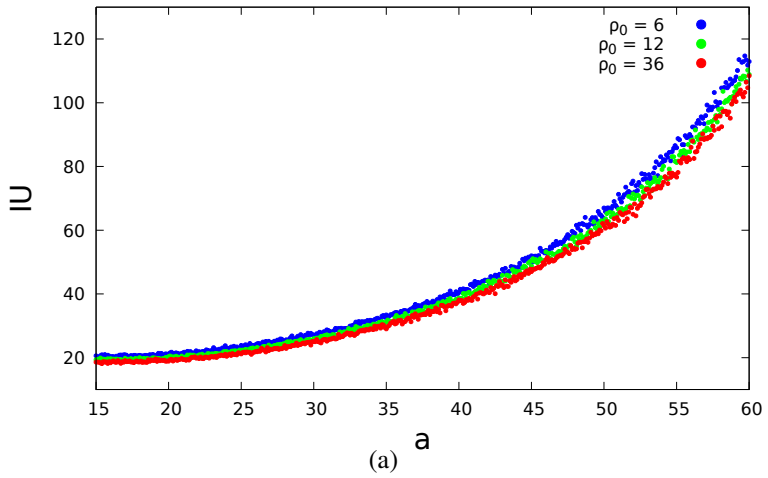

(a)

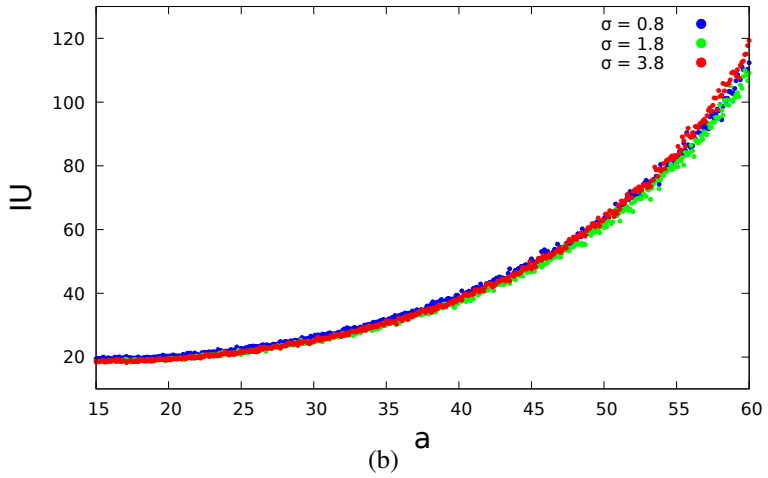

(b)

Figure 8: **The index of intensity use**. The index clearly increases for a decreasing bias, which means that the random walk becomes more and more tortuous, getting further and further away from a straight line. Several values of ρ_0 (top, setting $\sigma = 0.8$) and σ^2 (bottom, with $\rho_0 = 10$) for the single source of the system's arrangement depicted in Fig. 5 are also included. Every single dot depicted in this figure corresponds to a certain value of the index following the definition of Eq. 8.

of the width, though, has no remarkable effect, being therefore the tortuosity of the trajectories practically independent regarding how wide the source is.

4. Basins of attraction

The dynamical system comprised by the cell and the concentration sources has been designed through a discretized lattice. Each mesh node can be considered as an initial condition for a hypothetical random walk, and like any dissipative dynamical system, each one evolves in time and usually tends to a certain trapping region of space. In this work, the cell is attracted by a source, which behaves as an attractor of the system. Under these conditions, we can use the idea of basins of attraction for each attractor in order to classify every initial condition corresponding to the source by which the cell is captured [52, 53]. However, we have to distinguish a fundamental characteristic of this particular system: its dynamics is not essentially deterministic, but it is subject to the intrinsic randomness of the walks. This fact makes possible that any dynamic repetition in the same initial condition exhibits a different final state, that is to say, the cell is captured by another distinct source in comparison to the original case. Therefore, we can not trivially speak of a sensitivity to initial conditions, since its temporal evolution is, although biased, stochastic.

The cell is attracted by the higher values of the concentration potential. Then, the potential peaks located at the center of the sources behave as attractor points, geometrically speaking. Since initial conditions evolve haphazardly towards these points, we use a particular and simplified example of the so-called stochastic basins of attraction [38]. To study their appearance, we use the bistable system depicted in Fig. 1, with both attractor sources symmetrically situated in space. Although each of them slightly differs from its analogous in ρ_0 and σ^2, we approximate the deterministic boundary of the basins of each one splitting the whole space into two regions also in a symmetrical way. Indeed, and despite both sources being located at the same distance from the center of the map, this is an approximation, since the attraction intensity of each one is different from the other. Then, the resulting horizontal line, which separates both source regions of the corresponding attractors, contains initial conditions located exactly in the middle between the sources.

Considering the stochasticity and the lack of determinism of the dynamics of the random walks, the representation of these basins of attraction must be based on the probability of cellular capture by the attractor sources. Indeed, and as was mentioned before, if we repeat the simulation of a random walk that previously

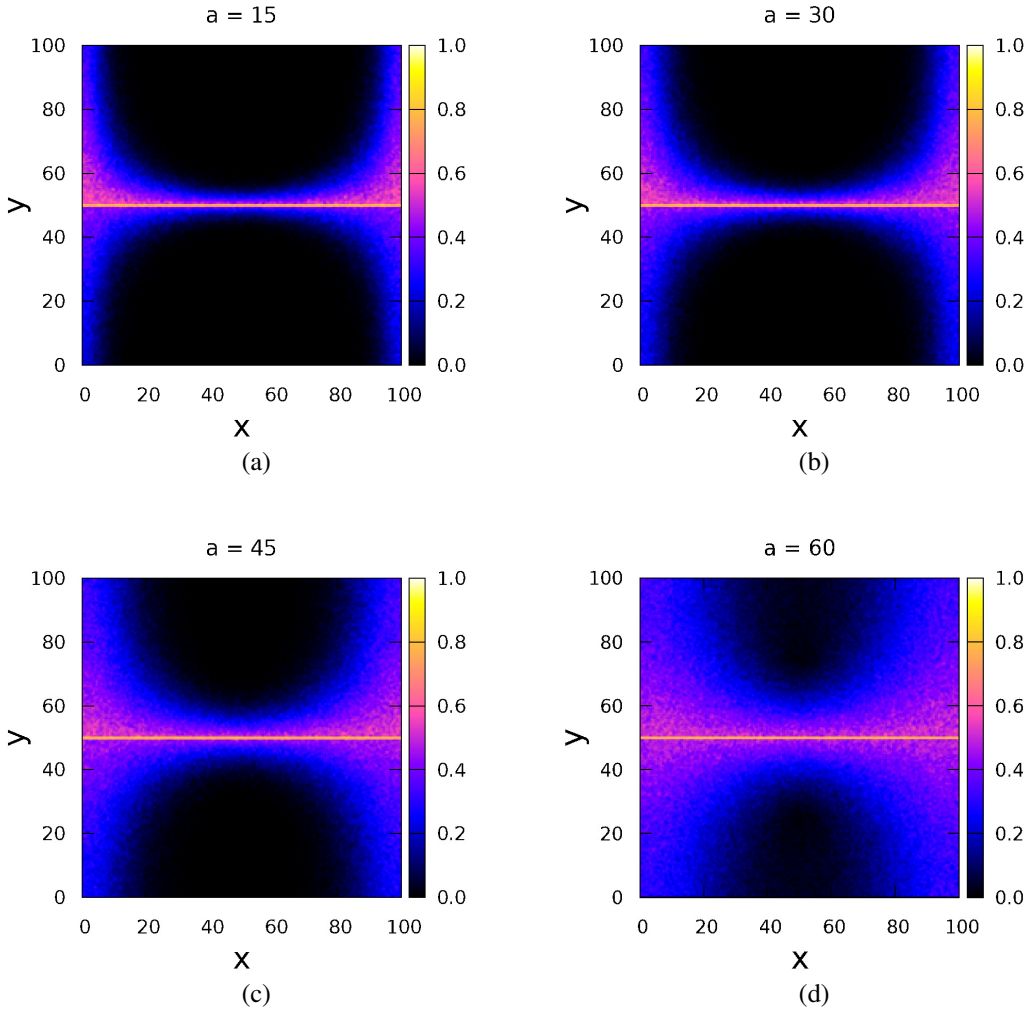

Figure 9: **Basins represented by probabilities**. Stochastic basins of attraction constructed through the definition of the probability of non-capture (colorbar). The two regions of the bistable system shown in Fig. 1 that contain one of both sources at the top and the bottom of the map, respectively, are clearly separated here by means of a horizontal line in the middle between them. Notice the different attraction of each source because of the different parameters shown in the definition of Eq. 3, being the lower one the most attractive. For an increasing value of a, and following the order (a), (b), (c) and (d), the bias becomes less intense and the probability increases. However, if we intensify it, the probability is almost zero in both regions, which means that the efficiency in cellular capture is very high.

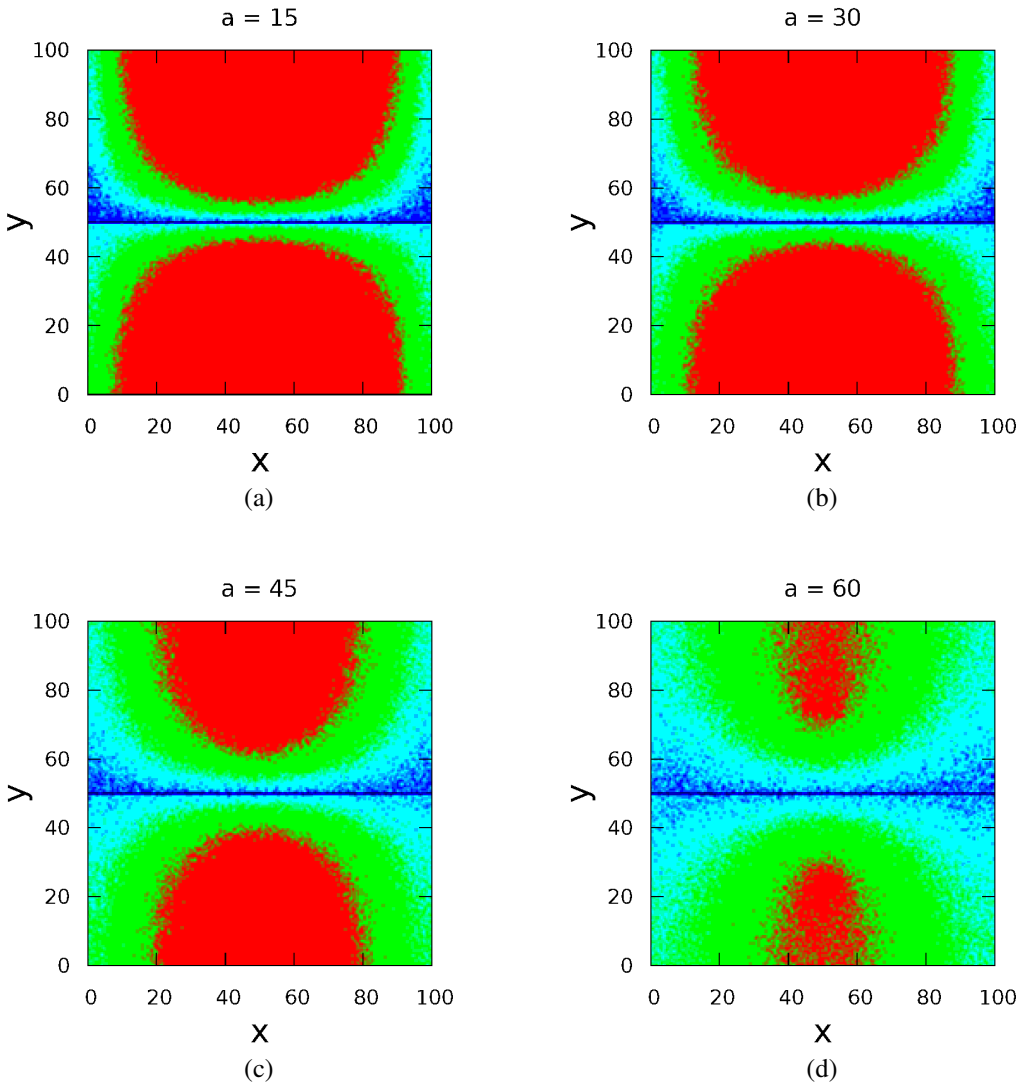

Figure 10: **Basins represented by thresholds**. Stochastic basins of attraction constructed through a threshold values definition, with $N < 5$ in red, with $5 \leq N < 30$ in green, with $30 \leq N < 50$ in cyan and with $N \geq 50$ in blue. For an increasing value of a, and following the order (a), (b), (c) and (d), we detect a progressive reduction of the extension of the red basin due to a less and less intense bias. However, if we intensify it, the basin of the corresponding source extends over almost the entire region, which means that the efficiency in cellular capture is very high.

was captured, now we can obtain another one that avoids its capture. It is noteworthy that the non-capture of a cell in the upper region can only be due to the capture by the other source in the lower region, and vice versa. Therefore, we build the stochastic basins of attraction by using the probability of avoiding the cellular capture by the source in the corresponding region [54, 55]. The computation of this probability is achieved by dividing the number of uncaptured cells N, with respect to the total number $N_T = 100$ of random walks performed for each initial condition. The results are displayed in Fig. 9 for different intensities of the bias.

Another representation of the stochastic basins that we have considered is through threshold values for these uncapturated cells: if $N < 5$ we paint the point in red, if $5 \leq N < 30$ in green, if $30 \leq N < 50$ in cyan and if $N \geq 50$ we use the blue color. The results are also displayed now in Fig. 10. We note that, for increasing values of parameter a, the non-capture probability increases correspondingly and, therefore, the red basin for $N < 5$ becomes smaller. If the bias is weaker, the possibility that a cell is not captured is larger, mainly far from the center of the source. This means that, even though the cellular attraction of both sources is less intense, the capture by the attractor in the other region becomes more likely than in conditions with lower a. On the other hand, for decreasing values of parameter a, this red basin expands through the corresponding region, being the biggest one with respect to the others defined by the different thresholds. This means that the bias turns to be almost deterministic, since its intensity is so large that strongly diminishes the non-capture probability. Therefore, we can say that the efficiency of the bias is very high, because most initial conditions of both regions represent a very poor probability that the cell avoids its capture by the corresponding source. As can be seen, the nonlinear bias function described in Eq. 7 behaves correctly and the concept of stochastic basins of attraction can be a very powerful tool to characterize the nature of this bias of the random walks in those environments in which the gradients are stationary or not changing very rapidly, in comparison with the speed of cell motion.

5. Conclusions and Discussion

We have designed a hybrid model of chemotactic cellular attraction using random walks on a lattice. A new and very easily constructed bias function that can be intensified through the variation of a single parameter has been devised. To this end, we have used the well-known Gompertz curve to construct the bias in a simple way. The solution of Poisson's equation has allowed us to relate the

chemical concentration of a certain substance in a medium with an effective potential, which has entailed us to model the attraction by the sources. A spatial discretization adapting the continuous partial differential equation to the discrete cell motion has been key for this purpose [17, 25, 30]. This aspect makes our hybrid chemotactic model computationally very affordable in comparison with those based on nonlinear partial differential equations [39]. They also make the model specially useful to be incorporated in previously designed hybrid cellular automata models that require very large computation times, and which are aimed at representing processes of lymphocyte recruitment in the description of tumor-immune cell interactions [26, 27, 28, 56].

We have studied how indexes of motion behavior [37] vary as a function of a single and simply accessible constant, analyzing the great impact that this intensity parameter has on the bias. Random walks traced by the cells subject to an increasing cellular attraction gain straightness in shape, and at the same time lose spatial sphericity. We have checked that the differences between the quantitative results obtained for different values of the bias parameter a are not proportional to the variation of the latter. Indeed, the increase or decrease of the different indexes of motion behavior is nonlinear with this variation, probably following an algebraic law like a power or an exponential one. This curvature makes the bias very sensitive to the variations of the parameter, which avoids using too large parameter domains.

To conclude, we have applied to chemotaxis the concept of stochastic basins of attraction [38] to pictorially analyze the attraction capability of each source with respect to the cell. The efficiency of the bias function has become clearer, since all random walks around an attractor are captured by it with high probability. Thus, the bias can be so weak that makes a captured cell's path too tortuous or, equivalently, so intense that makes its capture practically deterministic, despite the intrinsic randomness of the system.

6. ACKNOWLEDGMENTS

The authors wish to thank Laia Barjuan for helpful comments and discussions. This work was supported by the Spanish State Research Agency (AEI) and the European Regional Development Fund (ERDF, EU) under Project No. PID2019-105554GB-I00.

Conflict of interest

The authors declare that they have no conflict of interest.

CRediT authorship contribution statement

Jaume Ojer: Investigation, Visualization, Software, Formal analysis, Writing - original draft. **Álvaro G. López:** Supervision, Conceptualization, Investigation, Formal analysis, Writing - original draft. **Javier Used:** Supervision, Conceptualization, Investigation, Formal analysis, Writing - original draft. **Miguel A.F. Sanjuán:** Supervision, Conceptualization, Investigation, Formal analysis, Writing - review & editing, Funding acquisition.

References

[1] Engelmann TW. Neue Methode zur Untersuchung der Sauerstoffausscheidung pflanzlicher und thierischer Organism. Pfl Arch Ges Physiol Mens Tiere 1881;25:285-292.

[2] Pfeffer WF. Locomotorische Richtungsbewegungen durch chemische Reize. Unters Bot Inst Tübingen 1884;1:363-482.

[3] Sourjik V, Wingreen NS. Responding to chemical gradients: bacterial chemotaxis. Curr Opin Cell Biol 2012;24:262-268.

[4] Berg HC. Random walks in biology. Expanded ed. Princeton, N.J. : Princeton University Press; 1993.

[5] Adler J. Chemotaxis in bacteria. Science 1966;153:708-716.

[6] Benhamou S. Detecting an orientation component in animal paths when the preferred direction is individual dependent. Ecology 2006;87:518-528.

[7] Lux R, Shi W. Chemotaxis-guided movements in bacteria. Crit Rev Oral Biol Med 2004;15:207-220.

[8] Pearson K. The problem of the random walk. Nature 1905;72:294.

[9] Patlak CS. A mathematical contribution to the study of orientation of organisms. Bull Math Biophys 1953;15:431-476.

[10] Stevens A, Othmer HG. Aggregation, blowup and collapse: the ABC's of taxis in reinforced random walks. SIAM J Appl Math 1997;57:1044-1081.

[11] Saragosti J, Calvez V, Bournaveas N, Perthame B, Buguin A, Silberzan P. Directional persistence of chemotactic bacteria in a traveling concentration wave. Proc Natl Acad Sci USA 2011;108:16235-16240.

[12] Alt W. Biased random walk models for chemotaxis and related diffusion approximations. J Math Biol 1980;57:147-177.

[13] Hill NA, Häder DP. A biased random walk model for the trajectories of swimming micro-organisms. J Theor Biol 1997;186:503-526.

[14] Keller EF, Segel LA. Model for chemotaxis. J Theor Biol 1971;30:225-234.

[15] López ÁG. Dynamics in fractal spaces. Fractals 2021;29:2150016.

[16] Stevens A. The derivation of chemotaxis equations as limit dynamics of moderatly interacting stochastic many-particle systems. SIAM J Appl Math 2000;61:183-212.

[17] Charteris N, Khain E. Modeling chemotaxis of adhesive cells: stochastic lattice approach and continuum description. New J Phys 2014;16:025002.

[18] Othmer HG, Hillen T. The diffusion limit of transport equations II: Chemotaxis equations. SIAM J Appl Math 2002;62:1222-1250.

[19] Rivero MA, Tranquillo RT, Buettner HM, Lauffenburger DA. Transport models for chemotactic cell populations based on individual cell behaviour. Chem Eng Sci 1989;44:2881-2897.

[20] Hillen T, Painter KJ. A users guide to PDE models for chemotaxis. J Math Biol 2009;58:183-217.

[21] Guo Z, Tay JC. A hybrid agent-based model of chemotaxis. In: Shi Y, van Albada GD, Dongarra J, Sloot PMA, editors. Lecture notes in computer science. Computational Science - ICCS 2007. Springer, Berlin, Heidelberg; 2007, p. 119-127.

[22] Franz B, Xue C, Painter KJ, Erban R. Travelling waves in hybrid chemotaxis models. Bull Math Biol 2014;76:377-400.

[23] Lu H, Um K, Tartakovsky DM. Hybrid models of chemotaxis with application to leukocyte migration. J Math Biol 2021;82:1-28.

[24] Bilotta E, Pantano P. Cellular automata and complex systems: methods for modeling biological phenomena. 1st ed. IGI Global; 2010.

[25] Ferreira Jr SC, Martins ML, Vilela MJ. Reaction-diffusion model for the growth of avascular tumor. Phys Rev E 2002;65,021907.

[26] López ÁG, Seoane JM, Sanjuán MAF. Destruction of solid tumors by immune cells. Commun Nonlinear Sci Numer Simul 2017;44:390-403.

[27] López ÁG, Seoane JM, Sanjuán MAF. Dynamics of the cell-mediated immune response to tumor growth. Phil Trans R Soc A. 2017;375:20160291.

[28] Mallet DG, De Pillis LG. A cellular automata model of tumor-immune system interactions. J Theor Biol 2006;239:334-350.

[29] Tindall MJ, Porter SL, Maini PK, Gaglia G, Armitage JP. Overview of mathematical approaches used to model bacterial chemotaxis I: the single cell. Bull Math Biol 2008;70:1525-1569.

[30] Alber M, Chen N, Lushnikov PM, Newman SA. Continuous macroscopic limit of a discrete stochastic model for interaction of living cells. Phys Rev Lett 2007;99:168102.

[31] Othmer HG, Dunbar SR, Alt W. Models of dispersal in biological systems. J Math Biol 1988;26:263-298.

[32] Codling EA, Plank MJ, Benhamou S. Random walk models in biology. J R Soc Interface 2008;5:813-834.

[33] Stevens A. A stochastic cellular automaton modeling gliding and aggregation of myxobacteria. SIAM J Appl Math 2000;61:172-182.

[34] Muramatsu M, Nagatani T. Jamming transition in two-dimensional pedestrian traffic. Physica A 2000;275:281-291.

[35] Burstedde C, Klauck K, Schadschneider A, Zittartz J. Simulation of pedestrian dynamics using a 2-dimensional cellular automaton. Physica A 2001;295:507-525.

[36] Pillay S, Bryne HM, Maini PK. Modeling angiogenesis: A discrete to continuum description. Phys Rev E 2017;95:012410.

[37] Almeida PJAL, Vieira MV, Kajin M, Forero-Medina G, Cerqueira R. Indices of movement behaviour: conceptual background, effects of scale and location errors. Zoologia 2010;27:674-680.

[38] Serdukova L, Zheng Y, Duan J, Kurths J. Stochastic basins of attraction for metastable states. Chaos 2016;26:073117.

[39] Painter KJ. Mathematical models for chemotaxis and their applications in self-organisation phenomena. J Theor Biol 2019;481:162-182.

[40] Lin CC, Segel LA. Mathematics applied to deterministic problems in the natural sciences. 1st ed. Macmillan; 1974.

[41] Okubo A, Levin SA. Diffusion and ecological problems: modern perspectives. 2nd ed. Springer, NY; 2001

[42] Stefănescu R, Dura G. Numerical algorithms for a second order elliptic BVP. Annals of Alexandru Ioan Cuza University 2007;Tome LIII:103-118.

[43] Gerald CF, Wheatley PO. Applied Numerical Analysis. 7th ed. Pearson/Addison-Wesley; 2004.

[44] Nams VO. The VFractal: a new estimator for fractal dimension of animal movement paths. Landsc Ecol 1996;11:289-297.

[45] Dudley RM. Uniform central limit theorems. 2nd ed. Cambridge University Press; 2014.

[46] Lipowski A, Lipowska D. Roulette wheel selection via stochastic acceptance. Physica A 2012;391:2193-2196.

[47] Rudnick J, Gaspari G. Elements of the random walk: an introduction for advanced students and researchers. Illustrated ed. Cambridge University Press; 2004.

[48] Sciutto SJ. Study of the shape of random walks. II. Inertia moment ratios and the two-dimensional asphericity. J Phys A 1995;28:3667-3679.

[49] Benhamou S. How to reliably estimate the tortuosity of an animal's path: straightness, sinuosity, or fractal dimension?. J Theor Biol 2004;229:209-220.

[50] Hailey A, Coulson IM. Differential scaling of homerange area to daily movement distance in two African tortoises. Can J Zool 1996;74:97-102.

[51] Loretto D, Vieira MV. The effects of reproductive and climatic seasons on movements in the black-eared opossum (*Didelphis aurita* Wied-Neuwied, 1826). J Mammal 2005;86:287-293.

[52] Nusse HE, Yorke JA. Basins of attraction. Science 1996;271:1376-1380.

[53] Menck PJ, Heitzig J, Marwan N, Kurths J. How basin stability complements the linear-stability paradigm. Nature Phys 2013;9:89-92.

[54] Nieto AR, Seoane JM, Sanjuán MAF. Final state sensitivity in noisy chaotic scattering. Chaos Solitons Fractals 2021;150:111181.

[55] Nieto AR, Seoane JM, Sanjuán MAF. Noise activates escapes in closed Hamiltonian systems. Commun Nonlinear Sci Numer Simul 2021;105:106074.

[56] López ÁG, Seoane JM, Sanjuán MAF. Modelling cancer dynamics using cellular automata. In: Berezovskaya F, Toni B, editors. Advanced mathematical methods in biosciences and applications. STEAM-H: Science, Technology, Engineering, Agriculture, Mathematics & Health. Springer, Cham; 2019, p. 159-205.